doi:10.26443/seismica.v5i1.1953
SEISMICA

Does Episodic Tremor and Slip Influence Seismicity in Northern Cascadia?

Madison Bombardier * [1], **John F. Cassidy** [2,1], **Stan E. Dosso** [1]

[1]School of Earth and Ocean Sciences, University of Victoria, Victoria, Canada, [2]Geological Survey of Canada-Pacific, Natural Resources Canada, Sidney, Canada

Author contributions: *Data Curation*: Madison Bombardier. *Formal Analysis*: Madison Bombardier. *Methodology*: Madison Bombardier. *Writing - Original draft*: Madison Bombardier. *Writing - Review & Editing*: John F. Cassidy, Stan E. Dosso. *Visualization*: Madison Bombardier. *Funding acquisition*: John F. Cassidy.

Abstract This paper presents a spatial-temporal analysis of potential links between episodic tremor and slip (ETS) and seismicity in northern Cascadia. We define spatial-temporal clusters of tremor episodes to represent ETS between 2006 and 2024, and we merge six earthquake catalogues to represent regional seismicity. The statistical analysis focuses on seismicity rates and magnitude distributions of earthquakes throughout the mid-lower forearc crust and within the subducting plate. We find that in time periods between ETS events there exist fewer M $\gtrsim$ 2.5 earthquakes in/near the ETS zone than are predicted by a best-fit Gutenberg–Richter law (GR). During ETS and shortly afterwards, M $\gtrsim$ 2.5 earthquakes in close proximity to ETS events are slightly more numerous, such that seismicity is accurately represented by the GR law. Variations in earthquake magnitudes before ETS and during/after ETS are shown to be statistically significant, although the overall average occurrence rate of M $\gtrsim$ 2.5 earthquakes per ETS event is low, at 0.8 earthquakes per ETS event. We find no statistical evidence for temporal variations in daily seismicity rates (regional and proximal to ETS) in association with ETS. We discuss several challenges in the study of this topic in Cascadia, and highlight some instances that may warrant further investigation.

Production Editor:
Yen Joe Tan
Handling Editor:
Mathilde Radiguet
Copy & Layout Editor:
Tara Nye

Received:
August 18, 2025
Accepted:
June 12, 2026
Published:
TBD

Non-technical summary The Cascadia subduction fault hosts slow slip events that are associated with low-frequency seismic tremor, together called episodic tremor and slip (ETS). Previous work suggests there is an anti-correlation between the geographic distribution of ETS and regular earthquakes in Cascadia. Some other subduction zones exhibit increased rates of regular earthquakes seemingly in response to slow slip events. This paper presents a statistical analysis of ETS and regular earthquakes in northern Cascadia and examines whether earthquakes exhibit spatial and temporal variation associated with ETS. Our analysis finds that the magnitude distribution of earthquakes during ETS events and shortly afterwards contains more M $\gtrsim$ 2.5 earthquakes than the magnitude distribution of earthquakes occurring between ETS events. While this observation is statistically significant, the overall average occurrence rate of M $\gtrsim$ 2.5 earthquakes is low, at 0.8 earthquakes per ETS event. We find no statistical evidence for temporal variations in daily seismicity rates in association with ETS. We discuss several challenges in the study of this topic in Cascadia, and highlight some instances that may warrant further investigation.

1 Introduction and Background

Transient slow slip events, one type of slow earthquake, have been observed in many subduction zones (Dragert et al., 2001; Ozawa et al., 2001; Wallace et al., 2012; Schwartz and Rokosky, 2007), some transform boundaries (Linde et al., 1996; Wech et al., 2012), and even volcanic environments (Segall et al., 2006). Transient slow slip is generally recognized as an intermediate mode of slip between continuous creep and fast unstable slip that characterizes regular earthquakes. Slow slip can be aseismic or variably associated with low-frequency, low-amplitude seismic signals including tremor, low-frequency earthquakes, and very low-frequency earthquakes. While the mechanisms of these low-frequency seismic phenomena and their relationships are debated, it is known that they have different properties than regular earthquakes; thus, they are sometimes also referred to as slow earthquakes. Given the relatively long duration (days to years), small/moderate cumulative slip, and low stress drop of slow slip events, improvements in geodetic and seismic monitoring in recent decades have revealed a breadth of observations that increasingly suggest such events are common, frequent, and ubiquitous (Kirkpatrick et al., 2021).

While slow slip events do not present a direct seismic hazard, the nature of their relationship to regular, potentially-damaging earthquakes is a critical topic of study. If there is a causal relationship between slow and regular (fast) earthquakes—in particular, if slow earthquakes are found to reliably trigger regular earthquakes—it may facilitate short-term earthquake forecasting. Presently, it is thought that the frictional conditions that facilitate slow slip do not support regular earthquakes; which is to say, the areas on a fault that host slow and fast slip are largely mutually exclusive

*Corresponding author: madisonbombardier@gmail.com

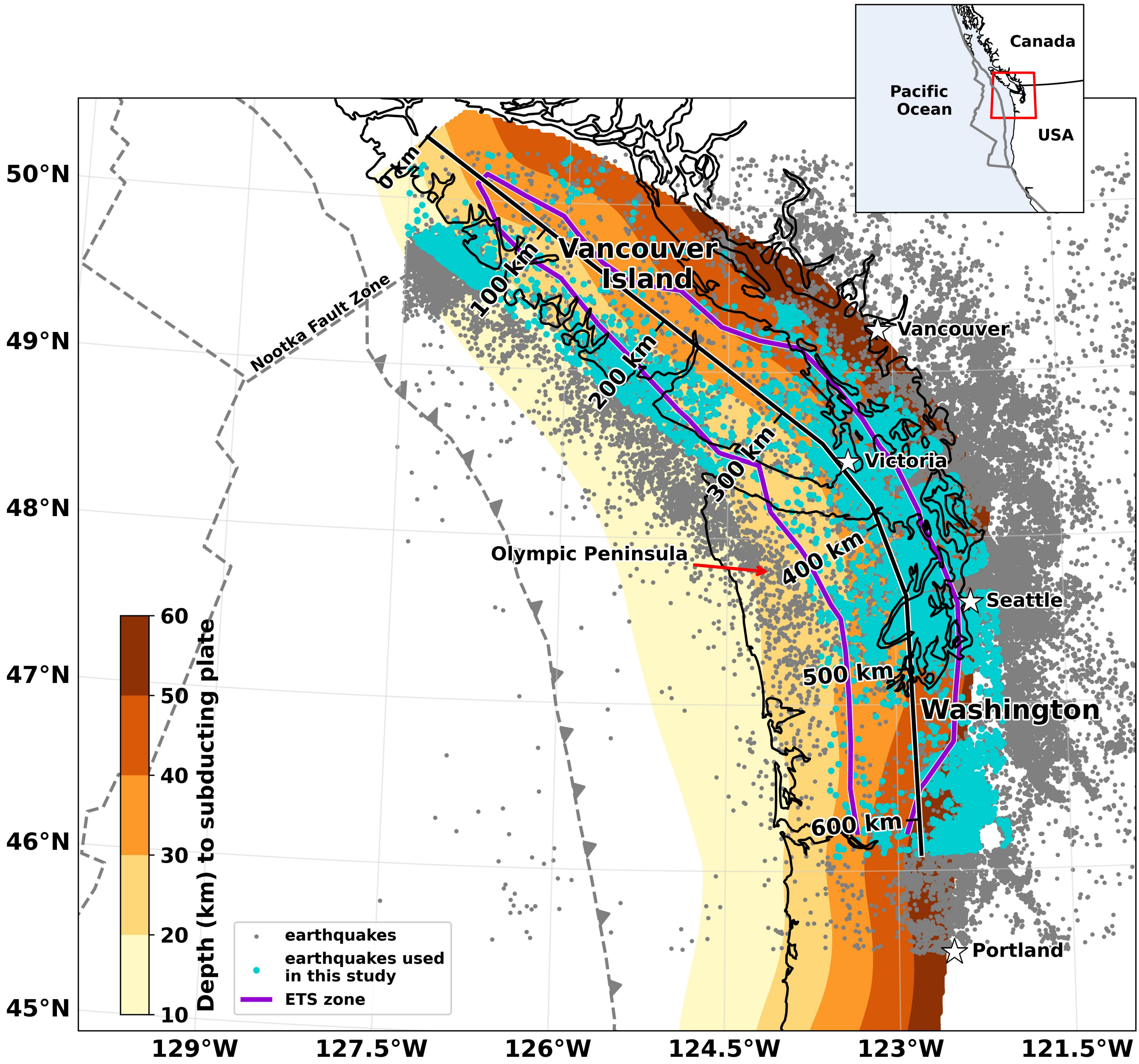

Figure 1 Map of the northern Cascadia area with seismicity, main tectonic features, and geographic references. Earthquakes in the entire combined catalogue (Section 2.2) between 1970 and 2024 are shown by grey dots, and the subset of earthquakes near the ETS zone used in this study are shown by blue dots. Purple line denotes the approximate ETS zone as the boundary containing 90% of tremor events used in this study. Orange shading represents the depth of the top of the subducting oceanic plate (Bloch et al., 2023). The black line along the margin denotes the transect used throughout. Dashed grey lines represent tectonic boundaries and major fault zones, including the subduction deformation front (with grey triangles). (inset) Broader geographic region with tectonic plate boundaries (grey lines), the political border between Canada and the USA (black line), and the study area (red polygon).

(e.g., Gao and Wang, 2017). As such, if slow earthquakes influence the occurrence of regular earthquakes, it is expected that some temporary perturbation would be transmitted spatially on a single fault (i.e., along dip or strike) and/or transferred to other faults. The most hazardous of such potential scenarios is the triggering of a large megathrust earthquake by a slow slip event adjacent to the seismogenic zone, as seems to have indeed been the case for the M9.0 2011 Tohoku earthquake (Kato et al., 2012).

The Cascadia subduction zone constitutes offshore and onshore areas between the Nootka Fault Zone near the northern extent of Vancouver Island (Figure 1) and the Cape Mendocino triple junction offshore of northern California. The portion of the subduction fault capable of hosting damaging megathrust earthquakes extends from the trench offshore nearly to the coast and has been essentially quiescent throughout modern seismic monitoring, with the exception of one small segment off the coast of Oregon state (Tréhu et al., 2008). This quiescence is interpreted to result from a fully-locked subduction interface at a late stage in its earthquake cycle (Davis et al., 2023). Onshore, west of the volcanic belt, transient slow slip events occur at intervals ranging between 6 and 20 months between the northern (Vancouver Island and northern Washington), central (southern Washington and northern Oregon), and southern (southern Oregon and northern California) segments (Brudzinski and Allen, 2007; Boyarko et al., 2015; Bombardier et al., 2024).

In northern Cascadia—the focus of this study—slow slip events recur at intervals of 10.5–15.5 months (Bombardier et al., 2024) and are reliably accompanied by tectonic tremor that roughly tracks the migration of the slow slip front (Wech and Bartlow, 2014; Hall et al., 2019). While the fundamental nature of the relationship between tremor and slow slip remains uncertain, their broad association has led to the phrase "episodic tremor and slip" (ETS) describing the combined phenomena (Rogers and Dragert, 2003). As such, tremor epicentres are often used to represent the spatial and temporal occurrence of slow slip to enable long-term study of ETS (e.g., Kao et al., 2009; Wech et al., 2009; Wech and Creager, 2011; Boyarko et al., 2015; Bartlow, 2020; Itoh et al., 2022). In this study, we use a catalogue of tremor episodes, which are defined as large spatial-temporal clusters of tremor epicentres, to represent ETS events over 18 years between 2006 and 2024.

Some studies have identified earthquakes in very close spatial and temporal proximity to slow slip events offshore central (Hirose et al., 2014) and southwest (Yamamoto et al., 2022) Japan, in the Kīlauea volcano in Hawaii (Segall et al., 2006), on the San Andreas fault in California (Linde et al., 1996), and offshore the North Island in the Hikurangi subduction zone (Delahaye et al., 2009; Nishikawa et al., 2021; Yarce et al., 2023). In some cases, slow slip on the subduction interface is purported to trigger earthquakes on upper-plate fault networks above subducted seamounts (Todd et al., 2018; Shaddox and Schwartz, 2019). In other cases, elevated seismicity rates are observed within the subducting plate before slow slip events, interpreted to be driven by pre-slow slip conditions/processes (Kita et al., 2021). In many of the aforementioned cases, earthquake occurrence rates increase in association with slow slip events, and such earthquakes tend to occur in swarms with burst-like behaviour. There are three mechanisms hypothesized to facilitate such seismic triggering, which are high fluid pressures, fluid migration away from the subducting plate, stress loading, and magma intrusion (Nishikawa et al., 2023); the latter is generally not applicable to slow slip in subduction zones.

To date, ETS in Cascadia has only been observed where the top of the subducting plate is between 25 km and 45 km depth (Figure 1). While offshore GNSS measurements are limited, long-term seafloor pressure measurements west of central Vancouver Island do not show signs of slow slip offshore (Davis et al., 2023). Some observations from Cascadia demonstrate a general anti-correlation between the geographic distributions of ETS and forearc seismicity (Kao et al., 2009; Bostock et al., 2019), whereas some other case studies have observed the presence of small in-slab earthquakes concurrent with ETS (e.g., Vidale et al., 2011). In this study, we present an analysis of the spatial and temporal relationship between ETS and seismicity near and within the northern Cascadia ETS zone over 18 years. The statistical analysis focuses on seismicity rates and magnitude distributions of all earthquakes in the mid–lower forearc crust and subducting plate occurring in proximity to ETS events. In particular, we examine whether and how earthquake occurrence rates and magnitudes vary in proximity to ETS, if at all. We also describe the challenges of studying this topic in Cascadia and outline considerations for future work.

2 Data and Methods

2.1 ETS catalogue

Tremor episodes, defined as spatial-temporal clusters of tremor epicentres, are used as a proxy for the spatial extent and duration of ETS events. The catalogue of tremor episodes employed here has been updated from the original version published by Bombardier et al. (2024) to include 993 episodes ranging in size from 10 to >13,000 tremor events between January 2006 and March 2024. This updated version is a superset of the original, with 97 additional episodes from the expanded time period. A comprehensive description of the data, methods, and analysis of tremor episodes can be found in Bombardier et al. (2024), and a brief overview of the creation of this new catalogue is provided here.

Tremor in Cascadia has been monitored continuously since January 2006 by Wech and Creager (2008) and Wech (2010) and catalogued at the Pacific Northwest Seismic Network (PNSN) Tremor Map webpage (https://www.pnsn.org/tremor). We project these tremor events onto the linearly-partitioned along-strike transect shown in Figure 1 to determine their position along strike. Due to the nature of using normal vectors for projecting points onto a line, tremor events in areas downdip on the outside angle where two segments join are not normal to either segment and are therefore not projected onto the transect at all. This results in three areas—at 335 km, 388 km, and 453 km along strike—where tremor events (and earthquakes) are not considered in this study.

Tremor events that are successfully projected onto the transect are clustered using the density-based spatial clustering of applications with noise (DBSCAN) algorithm (Ester et al., 1996) in the along-strike/time domain. This process essentially defines an episode as a minimum of 10 tremor events with a mutually-exclusive maximum of 3 days or 20 km along strike between neighbouring events. Tremor episodes containing ≥1,500 events are considered to represent ETS events. Since there is no standard definition of ETS, this simple but effective rubric is chosen to produce a set of episodes that conform with previously-published literature (Bombardier et al., 2024). There are 37 episodes that meet this criterion and are therefore considered to

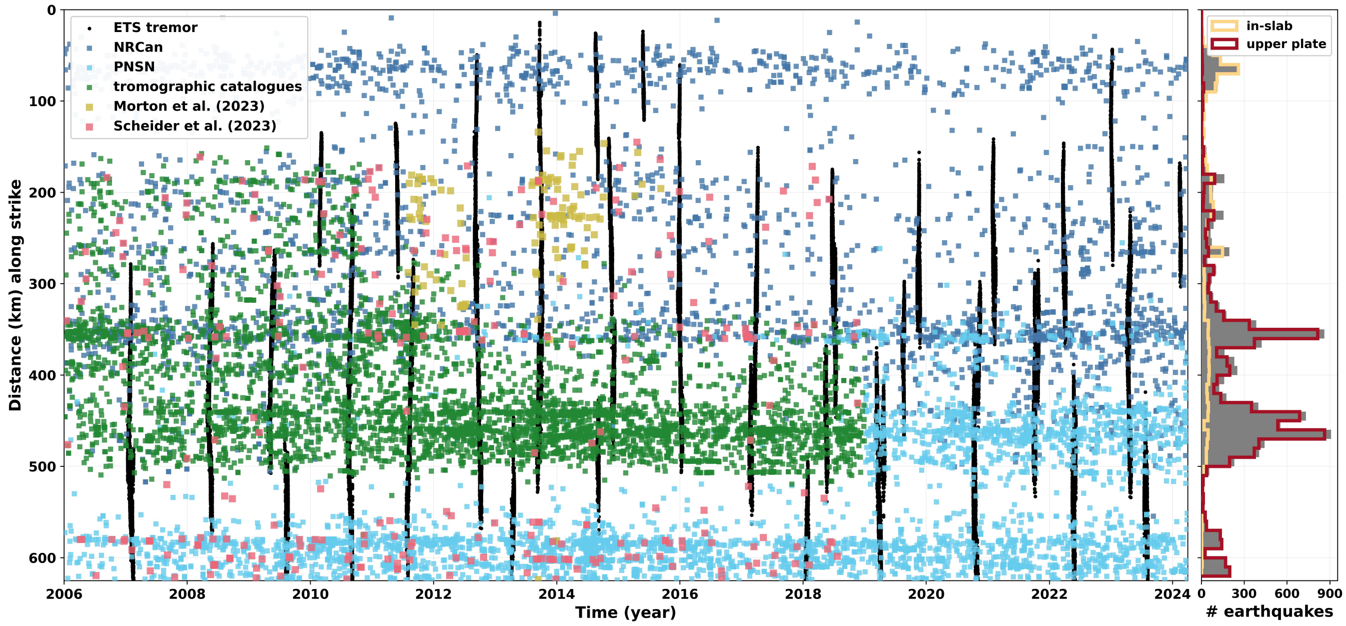

Figure 2 Earthquakes (squares) near the ETS zone used in this study along strike over time coloured according to which catalogue provided their location solution. Histograms on the right show the total number of earthquakes along strike (grey bars) and the subsets that have depths shallower (red line) and deeper (yellow line) than the top of the oceanic crust modelled by Bloch et al. (2023). These earthquakes are the same set shown as blue dots in Figure 1. ETS events are represented by tremor (clustered black dots appearing as vertical lines).

represent ETS events in this study (Figure 2).

Smaller tremor episodes, so-called inter-ETS events, are comprehensively characterized by Bombardier et al. (2024) but have otherwise been understudied. Their short durations (a few days) and deep centroids usually preclude slip modelling using diurnal GNSS observations, but it is expected that slow slip does occur during such events (Wech and Creager, 2011; Bartlow, 2020). Work focused in the Hikurangi subduction zone indicates that slow slip events with larger cumulative slip are associated with larger seismicity rate increases (Todd et al., 2018). Given the difficulty of modelling slip of small ETS events, and given that larger events are more likely to be associated with noticeable changes in seismicity, we exclude inter-ETS events (956 tremor episodes) from our analysis. The full tremor episode catalogue provides information such as start/end times and along-strike extent that is publicly available on Zenodo (Bombardier, 2025).

2.2 Earthquake catalogues

Regular earthquakes in the region are routinely catalogued by Natural Resources Canada (NRCan) and PNSN. Since northern Cascadia straddles the Canada-USA border, a catalogue of regional seismicity requires integration of the official NRCan and PNSN catalogues. We use three original catalogues of earthquakes in the northern Cascadia region computed by Morton et al. (2023), NRCan, and PNSN, plus three catalogues (described below) that provide metadata (Schneider et al., 2023) or relocated hypocentres (Savard et al., 2018; Merrill et al., 2020) for events in the NRCan and PNSN catalogues. Table 1 gives the number of events contributed by each catalogue and the time period and region for which they apply, and Figure 2 shows all earthquakes that are used in this study along strike over time (same as blue dots in Figure 1). We first scan these catalogues individually for duplicates by identifying any pair of events that have origin times within 3 s and epicentres within 15 km. Where duplicates are identified, the earlier event is kept as an arbitrary standard; it would be ideal to use some measure of uncertainty to determine which event to keep, but this information is not provided for all catalogues and we prefer a method that can be applied uniformly.

We then combine the catalogues in a series wherein duplicate events are identified with the integration of each new catalogue. We begin by integrating the NRCan catalogue with the PNSN catalogue. Duplicates between catalogues are identified using the aforementioned conditions (within 3 s and 15 km), and the NRCan solution is prioritized. Additional catalogues are integrated into this combined catalogue using the same conditions for handling duplicates, and priority is granted to the new catalogue that is being integrated at that stage. In this way, the order of integration (the same order given in Table 1) represents a prioritization hierarchy for duplicate events.

The NRCan and PNSN catalogues provide the foundation of our combined earthquake catalogue. The NRCan catalogue is a combination of the National Earthquake DataBase (NEDB) and the Seismic Hazard Earthquake Epicentre File (SHEEF) (Halchuk et al., 2015). The SHEEF is a version of the NEDB that has been processed for use in Canada's fifth generation seismic hazard model; it contains events M $\geq$ 2.5 up to 2010, whereas the NEDB contains all located seismic events, including non-tectonic activity, up to March 2024. As

Original Catalogue	Number of Events	Time Range	Geographic Region
PNSN	4,395	January 2006–March 2024	Washington (USA)
NRCan	3,241	January 2006–March 2024	Vancouver Island (Canada)
Morton et al. (2023)	140	July 2011–October 2015	northern Cascadia (Canada and USA)
Schneider et al. (2023)	285	January 2006–December 2018	northern Cascadia (Canada and USA)
Savard et al. (2018)	1,143	January 2006–May 2012	Vancouver Island (Canada)
Merrill et al. (2020)	3,642	January 2006–December 2018	Washington (USA)
Combined total	12,846	January 2006–March 2024	northern Cascadia (Canada and USA)

Table 1 Earthquakes in the combined earthquake catalogue between January 2006 and March 2024 within 60 km of the along-strike transect and the catalogue from which the location solution originates. Note that Schneider et al. (2023)'s Pacific Northwest catalogue contributes metadata for 756 earthquakes, but location solutions for only 285.

such, NEDB contributes events $M < 2.5$ before the end of 2010, and all events after 2010. The PNSN catalogue is accessed through a search of the earthquakes database on the PNSN website where we obtain all events up to March 2024.

A short-duration catalogue computed by Morton et al. (2023) uses automatic detection within a temporary ocean-bottom seismometer array to locate previously-unknown earthquakes along the Cascadia margin coastline. This catalogue is complete to approximately M1.9 between July 2011 and October 2015, and approximately 75% of events in this margin-wide catalogue are new detections.

The Pacific Northwest catalogue from Schneider et al. (2023) contains known events $M \geq 2.0$ up to 2018 from authoritative sources in the region, including NRCan and PNSN, and supplies metadata on earthquake swarms and aftershock sequences. Aftershock sequence identification is particularly important because such events are not expected to be related to slow slip, and even a handful of aftershocks can significantly temporarily affect regional seismicity rates. Events from this catalogue are removed if they are "likely/maybe" or "definitely" aftershocks (where the *scheme2020* variable is 4 or 5), which removed 40 aftershocks within the study period and area. Events are also removed if there is another reason the authors recommend their removal (such as being a duplicate) according to the *removal* variable. Aftershocks occurring beyond the time range of this catalogue (i.e., after 2018) are not identified and remain in this analysis. Note that this catalogue contributes event metadata for a total of 756 events used in this study, but contributes location information for only 285 events (Table 1 and Figure 2) because location information is replaced by that in the tomographic catalogues, described forthwith.

Two catalogues of earthquakes relocated in tomographic inversion by Savard et al. (2018) and Merrill et al. (2020) provide hypocentres for this study. The Savard et al. (2018) catalogue contains a relocated subset of the NRCan catalogue in the Vancouver Island region up to May 2012, and the Merrill et al. (2020) catalogue contains a relocated subset of the PNSN catalogue in the Washington region up to 2018. Events relocated through tomographic inversion are expected to have better depth constraints, which aid analysis of subduction interface proximity. If duplicates are identified during the integration of these catalogues, we keep only hypocentral information in order to preserve metadata that may exist from previously-integrated catalogues.

The resulting combined catalogue is truncated between January 2006 and March 2024 to be consistent with the time range of ETS observations. Earthquakes that are unlikely to be influenced by ETS are removed. These include events with depths deeper than 25 km below the top of the subducting plate and shallower than 10 km below sea level. We represent the top of the subducting oceanic crust as the "c-horizon" in the three-boundary subduction zone model estimated from receiver-function inversion by Bloch et al. (2023). We also remove earthquakes farther than 60 km orthogonal distance from the along-strike transect shown in Figure 1. The remaining earthquakes form the catalogue of 12,846 events shown in Figure 2 employed in this study (also shown as blue dots in Figure 1 and summarized in Table 1). Note that there are three under-resolved areas downdip of the transect at 335 km, 388 km, and 453 km where there are no orthogonal projections to the transect. These areas include an estimated 250 events ($<$ 2% of the total) that would have otherwise been included in this analysis.

We estimate the magnitude of completeness and b-value of the GR law fit to the combined catalogue containing all earthquakes (grey dots in Figure 1) and the subset near the ETS zone used in this analysis (blue dots in Figure 1) shown in Figure 3. The magnitude of completeness is estimated using the goodness-of-fit test (Wiemer and Wyss, 2000), which computes the lowest magnitude for which the observed cumulative frequency–magnitude distribution adequately fits the GR law predicted for the given distribution. In this case, an adequate fit is considered to be a sum of the absolute residuals between the observed cumulative distribution and associated GR law that is below 5% of the sum over the observed cumulative distribution. The b-value of the GR law associated with the magnitude of completeness is estimated using the maximum-likelihood method (Aki, 1965) and standard error estimate (Shi and

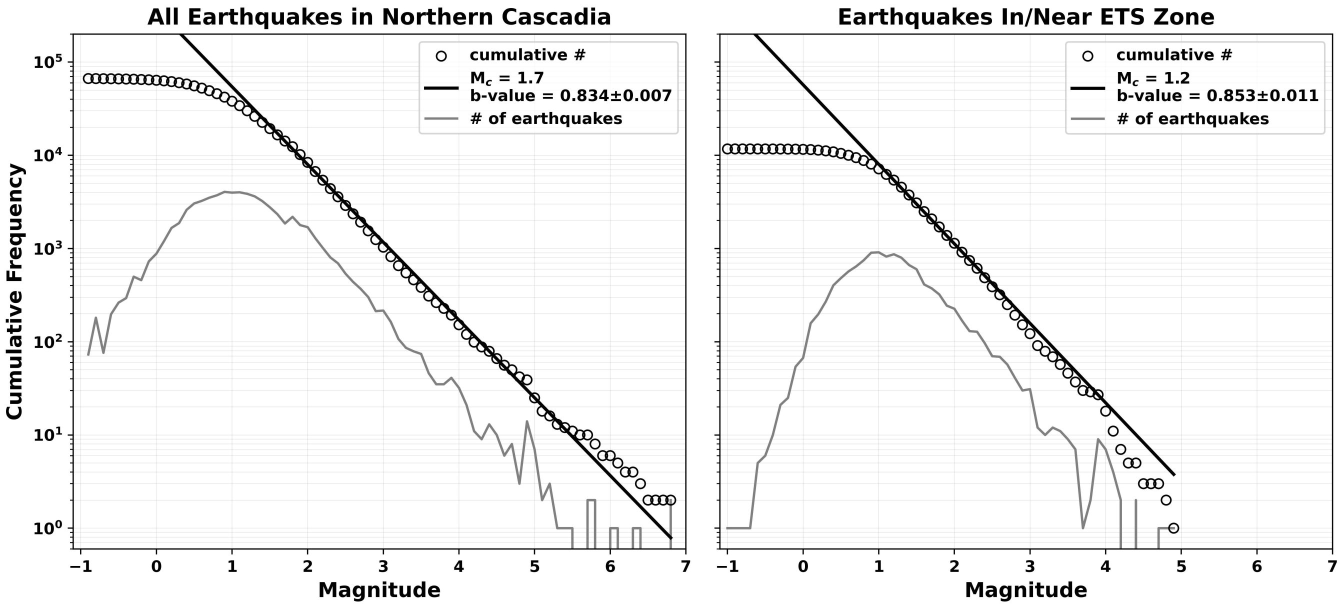

Figure 3 Cumulative frequency–magnitude distribution and Gutenberg–Richter (GR) law of earthquakes throughout northern Cascadia in the combined catalogue (left) and in the subset near the ETS zone (right). In Figure 1, the entire combined catalogue is shown as grey dots, and the subset near the ETS zone is shown as blue dots.

Bolt, 1982).

The magnitude of completeness for earthquakes in the combined catalogue in or near the ETS zone is lower at M1.2 than that for earthquakes throughout northern Cascadia at M1.7 (Figure 3). The ETS zone encompasses higher seismograph network density compared to areas farther inland and offshore, which likely accounts for its lower magnitude of completeness. The combined catalogue in/near the ETS zone is over estimated by the GR law for earthquakes M $\gtrsim$ 2.5, where the magnitude distribution appears to be slightly tapered towards low values. Earthquakes near the ETS zone exhibit a slightly higher *b*-value at 0.853$\pm$0.011 compared to that associated with all earthquakes throughout northern Cascadia at 0.834$\pm$0.007; however, detailed consideration of the *b*-value of a distribution that is not well described by the GR law may not be justified. Broadly, these observations indicate that earthquakes in/near the ETS zone are detected to lower magnitudes than those throughout the entire region and lack earthquakes M $\gtrsim$ 2.5 compared to the GR law expectation. In the 18 years of seismicity included in this analysis, no earthquake larger than M4.9 occurred in/near the ETS zone.

2.3 Defining spatial-temporal windows

To examine whether seismicity changes in relation to ETS, spatial-temporal windows are defined as before, during, after, and in-between ETS events. Seismicity within the same window types are aggregated over all ETS events and considered one dataset. Variation in seismicity rates—quantified as daily earthquake occurrence (DEO) by simply counting the number of earthquakes each day—and magnitude distributions between windows are assessed for statistical significance. Two test cases are considered and described below.

First, we compare seismicity during and between ETS using earthquakes in/near the ETS zone along the entire transect (blue dots in Figure 1). Days wherein ETS tremor occurs anywhere in northern Cascadia are considered ETS periods, and all other days are considered inter-ETS periods, as illustrated in Figure 4a for a one-year period. Any pair of ETS events overlapping in time are considered one event; there are three such pairs, including two examples shown in Figure 4a. As such, this test case considered 34 distinct time periods that are considered ETS periods. While it is not expected that, for example, seismicity near the southern limit of northern Cascadia would be related to ETS near the northern limit, there are no logical spatial boundaries that can be applied to inter-ETS periods without creating a bias. As such, this test provides a crude baseline of seismicity during and between ETS events.

Second, we compare seismicity within a maximum of 28 days before ETS, during ETS, and a maximum of 28 days after ETS using only earthquakes within the along-strike vicinity of each ETS event, as illustrated in Figure 4b for a one-year period. In this test case, the along-strike vicinity of a given ETS event includes the entire along-strike extent of the event (northernmost to southernmost tremor epicentres) plus 25 km beyond the extent in both directions along the transect. Any pair of ETS events overlapping in space and time within these bounds ($\pm$28 days and $\pm$25 km) are considered one event; there are six such pairs, including one example shown in Figure 4b. As such, this test case considers 31 distinct time periods for which seismicity before, during, and after ETS are compared.

Yarce et al. (2023) show that elevated earthquake occurrence rates interpreted to be due to a slow slip event in Hikurangi increase during the event and remain elevated for 1–2 weeks afterwards. As such, if seismicity responds similarly to ETS in northern Cascadia, we would expect higher DEO during and after ETS compared to

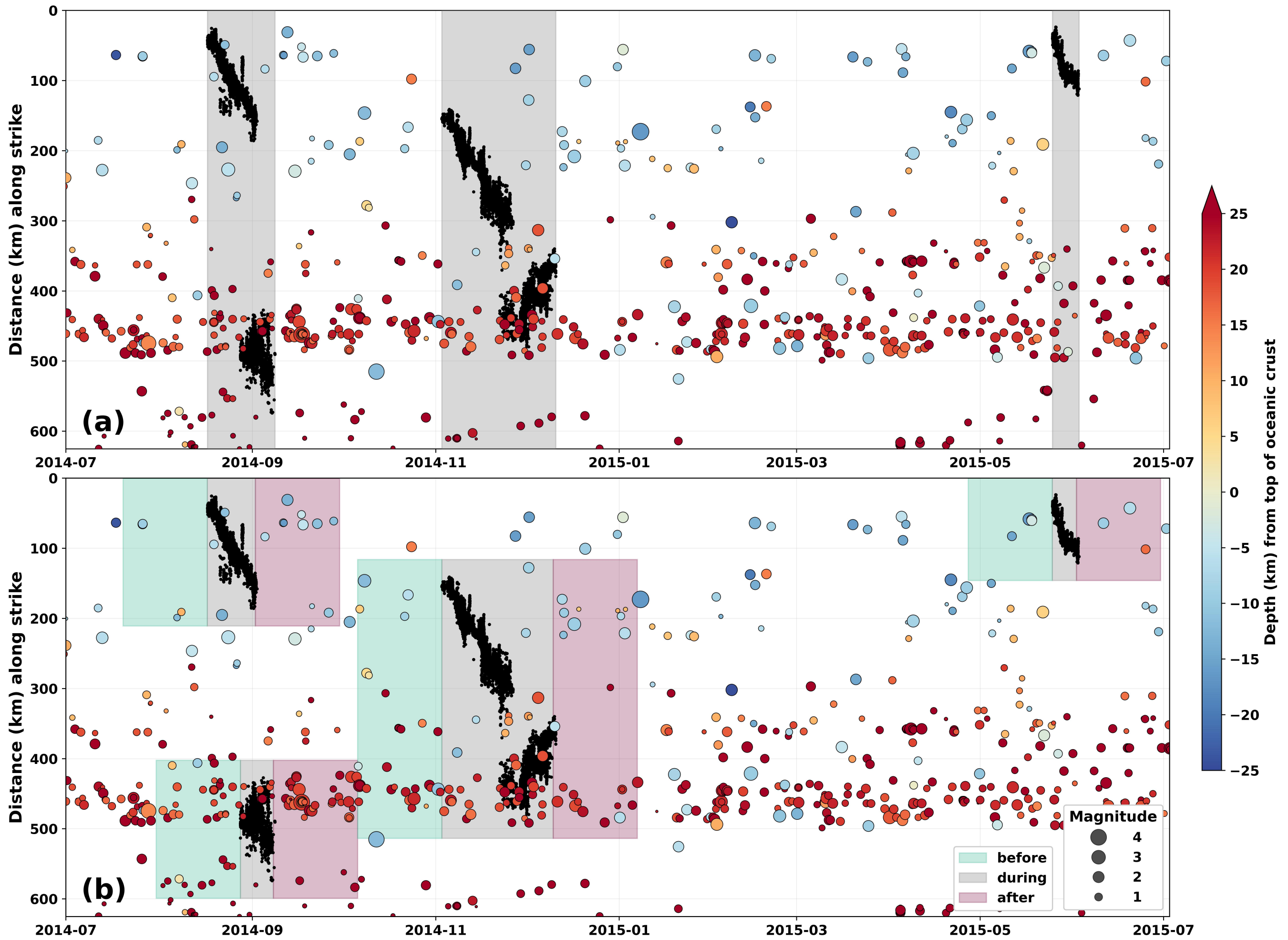

Figure 4 An example of spatial-temporal windows considered in relation to ETS. ETS tremor (black dots) and earthquakes (circles) coloured according to their depth from the top of the subducting plate model between July 2014 and July 2015. (a) Grey shaded windows encompass tremor and earthquakes considered to have occurred in ETS periods described in Section 3.1. Earthquakes outside of shaded windows are considered to have occurred in inter-ETS periods. (b) Green, grey, and purple shaded windows encompass tremor and/or earthquakes considered to have occurred before, during, and after ETS, respectively, described in Section 3.2.

before. The choice to define the before and after ETS periods as 28 days aligns with findings from Yarce et al. (2023) but are also somewhat arbitrary, so we therefore repeat this analysis (in supplementary materials) considering these periods to consist of 21, 14, and 7 days.

3 Results

3.1 Regional seismicity in ETS and inter-ETS periods

Figure 5 shows a histogram of DEO in ETS and inter-ETS periods. There are 1,486 earthquakes occurring over 833 days in ETS periods, for an average of 1.78 earthquakes per day. There are 11,244 earthquakes occurring over 5,815 days in inter-ETS periods, for an average of 1.93 earthquakes per day. Because inter-ETS periods include more days and more earthquakes than ETS periods, DEO frequency in Figure 5 is represented as a percentage of the total days in each period. In both ETS and inter-ETS periods, the frequency of days with progressively higher DEO decreases roughly exponentially as DEO increases. Visually, the distributions of DEO during and between ETS events shown in Figure 5 are similar, with the largest differences occurring for days where zero and two earthquakes occurred (Figure 5b), which represent differences of approximately 3.5% (DEO of 0) and -2% (DEO of 2) of days between ETS and inter-ETS periods.

A Kolmogorov–Smirnov (KS) test is used to determine whether the two datasets presented in Figure 5 are statistically distinct by testing whether the null hypothesis is falsified. In this case, the null hypothesis is that the two datasets are sampled from the same distribution and any differences are due to random variations. To falsify the null hypothesis, the resulting p-value must be sufficiently small—usually taken to be ≤ 0.05. Falsifying the null hypothesis is evidence that differences between two datasets are unlikely (i.e., $\leq 5\%$ probability) to be entirely due to random variations in sampling, and hence the implication is that the differences are likely due to distinct mechanisms/processes. A KS test performed on the DEO datasets represented in Figure 5

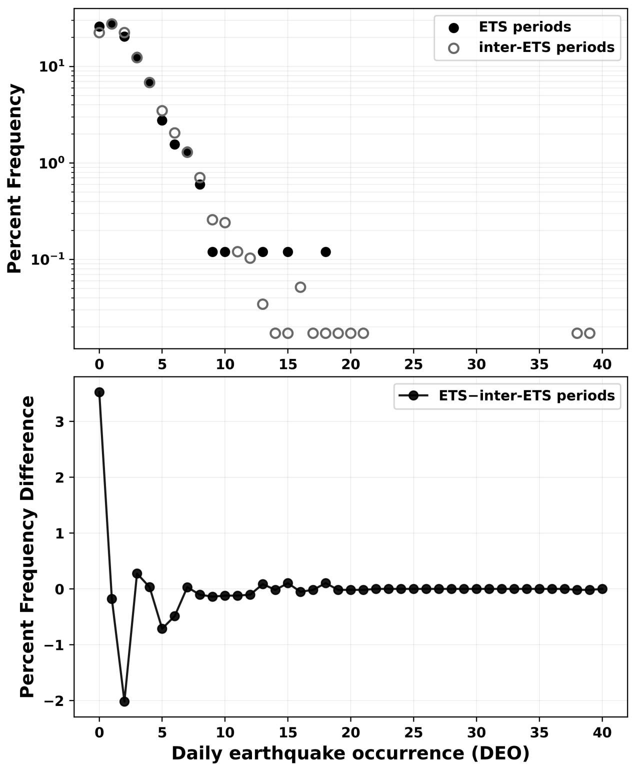

Figure 5 Distribution and comparison of daily earthquake occurrence (DEO) in ETS periods (black circles) and inter-ETS periods (grey open circles). (top) Histogram of DEO in each group shown as a percentage of the total days in each group. Only non-zero DEO values are shown. (bottom) Difference in percent frequency of DEO in the top panel.

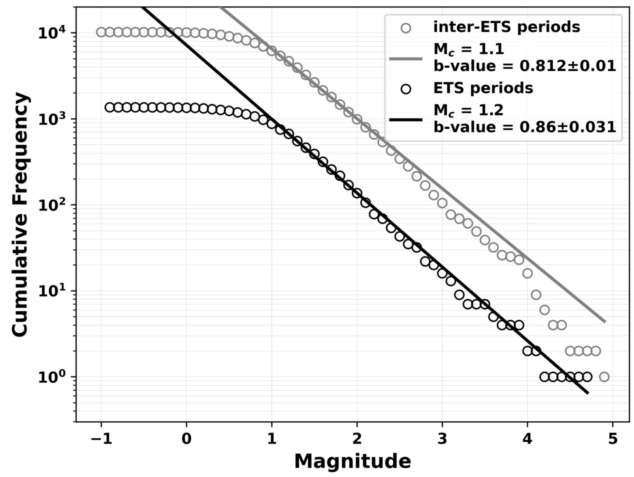

Figure 6 GR frequency–magnitude relationship (solid lines) fit to the cumulative frequency–magnitude distribution of earthquakes in inter-ETS periods (grey open circles) and ETS periods (black open circles).

fails to falsify the null hypothesis with a p-value of 0.32. In other words, differences in seismicity rates near the ETS zone in northern Cascadia (Figure 1) during and between ETS events are not interpreted to be geophysically meaningful.

The GR frequency–magnitude relationships representing earthquakes in ETS and inter-ETS periods are shown in Figure 6. The magnitude of completeness and b-value for inter-ETS periods are M1.1 and 0.812±0.010, and for ETS periods are M1.2 and 0.860±0.031. The cumulative magnitude distribution of inter-ETS earthquakes periods (grey circles in Figure 6) appears slightly tapered below the GR line for M $\gtrsim$ 2.5, whereas that representing ETS periods exhibits no such tapering. As discussed in Section 2.2, earthquakes M $\gtrsim$ 2.5 near the ETS zone over the entire study period are also slightly tapered below the best-fit GR line (Figure 3); categorizing these earthquakes as occurring in either ETS or inter-ETS periods (Figure 6) indicates that the tapering is dominantly driven by earthquakes occurring in inter-ETS periods. Since inter-ETS earthquakes do not strictly follow the GR law, their associated b-value should be considered with caution. A KS test performed on earthquake magnitudes in ETS and inter-ETS periods indicates weak evidence of a meaningful geophysical distinction between magnitude distributions, with a p-value of 0.061.

3.2 Proximal seismicity before, during, and after ETS

Figure 7 shows a histogram of DEO in the vicinity of ETS occurring within 28 days before ETS, during ETS, and 28 days after ETS, as well as the differences of DEO frequency. There are 868 days in the “before” and “after” ETS periods, within which 1,035 and 955 earthquakes occurred for an average of 1.19 and 1.14 earthquakes per day, respectively. During ETS events there are 903 days and 1,071 earthquakes, for an average of 1.19 earthquakes per day.

A KS test is performed on all pairs of DEO datasets, and the results are summarized in Table 2. The KS test performed on DEO during and before ETS yields a p-value of 0.99, indicating no evidence that the distributions are distinct. Tests on DEO during and after ETS, and on DEO before and after ETS, yields p-values of 0.66 and 0.64, respectively, giving no evidence that the distributions are distinct. Taken together, these results indicate no evidence of statistically-significant variation in rates of proximal seismicity before, during, and after ETS events.

The GR laws representing earthquakes before, during, and after ETS are shown in Figure 8. The estimated magnitudes of completeness are between M1.1 and M1.2, and b-values are between 0.811 and 0.878, with before ETS seismicity exhibiting the highest b-value and after ETS seismicity exhibiting the lowest. With a standard error of 0.036 on all b-values, the lowest and highest b-values are within the range of error of each other. In this case, as in Section 3.1 (Figure 6), tapering below the GR line for earthquakes M $\gtrsim$ 2.5 occurs before ETS but not during; it is inconclusive whether earthquakes occurring after ETS exhibit a taper. A KS test performed on earthquake magnitudes between each period indicates that earthquake magnitudes before ETS are statistically distinct from those during and after ETS, with p-values < 0.05 in both cases (Table 2). Correspondingly, earthquake magnitudes during/after ETS give a p-value

Periods	DEO test *p*-value	Magnitude test *p*-value
During/Before	0.99	0.02
During/After	0.66	0.68
Before/After	0.64	0.03

Table 2 Kolmogorov–Smirnov (KS) test *p*-value results for test cases involving DEO in the vicinity of ETS occurring within 28 days before ETS, during ETS, and 28 days after ETS. Low *p*-values indicate a greater probability that the two datasets are statistically distinct.

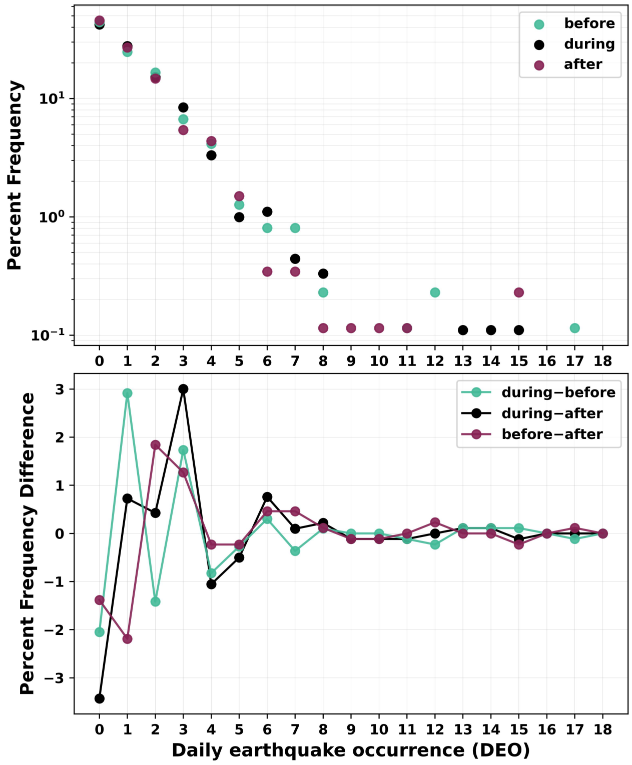

Figure 7 Distribution and comparison of daily earthquake occurrence (DEO) in three distinct time periods: before (green circles), during (black circles), and after (purple circles) ETS events. (top) Histogram of DEO in each group over all ETS events shown as a percentage of the total days in each group. Only non-zero DEO values are shown. The results of Kolmogorov–Smirnov (KS) tests performed on each pair of datasets are given in Table 2. (bottom) Difference in percent frequency of DEO in the top panel.

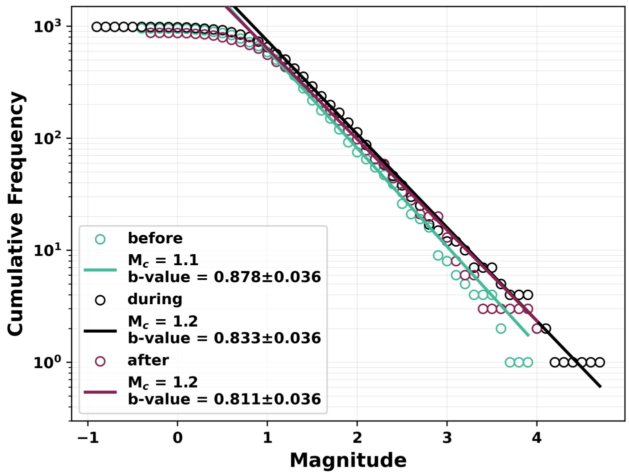

Figure 8 GR frequency–magnitude relationship (solid lines) fit to the cumulative frequency–magnitude distribution of earthquakes in three distinct time periods: before (green open circles), during (black open circles), and after (purple open circles) ETS events. The results of KS tests performed on each pair of datasets are given in Table 2.

of 0.68, indicating no distinction between the two sets. These results indicate that rates of proximal seismicity do not vary significantly in the weeks before, during, or after ETS events, but that the magnitudes of proximal seismicity do exhibit statistically-significant variations.

We repeat the analysis presented in this section considering time periods before and after ETS consisting of 21, 14, and 7 days instead of 28 days. This work is presented in supplementary materials Figures S1–S6 and Tabs S1 and S2. These results show similar patterns to those presented in the main text and support the interpretations made here.

4 Limitations and considerations for future work

In Section 3, we used observations over 18 years (2006–2024) to show that regional and proximal seismicity rates exhibit no significant temporal trends in relation to ETS, but that temporal differences in earthquake magnitude distributions are statistically significant. Specifically, we found that: (1) the frequency–magnitude distribution of regional seismicity in inter-ETS periods falls below the GR law (i.e., is tapered) for $M \gtrsim 2.5$; in contrast, seismicity in ETS periods is not tapered (Figure 6); and (2) the frequency–magnitude distribution of proximal seismicity before ETS is characterized by a slight taper for $M \gtrsim 2.5$, whereas proximal seismicity during and after ETS does not (Figure 8). In other words, earthquakes in/near the ETS zone have a background state characterized by fewer earthquakes $M \gtrsim 2.5$ than is predicted by the GR law. During ETS events and for a short time afterwards, a greater proportion of $M \gtrsim 2.5$ earthquakes occur such that the observed frequency–magnitude distribution better matches the GR law.

Statistical evidence of variations in earthquake magnitude distributions between ETS and inter-ETS periods is weak (*p*-value of 0.06; Section 3.1) but is strong before and during/after ETS (*p*-values of 0.02 and 0.03, re-

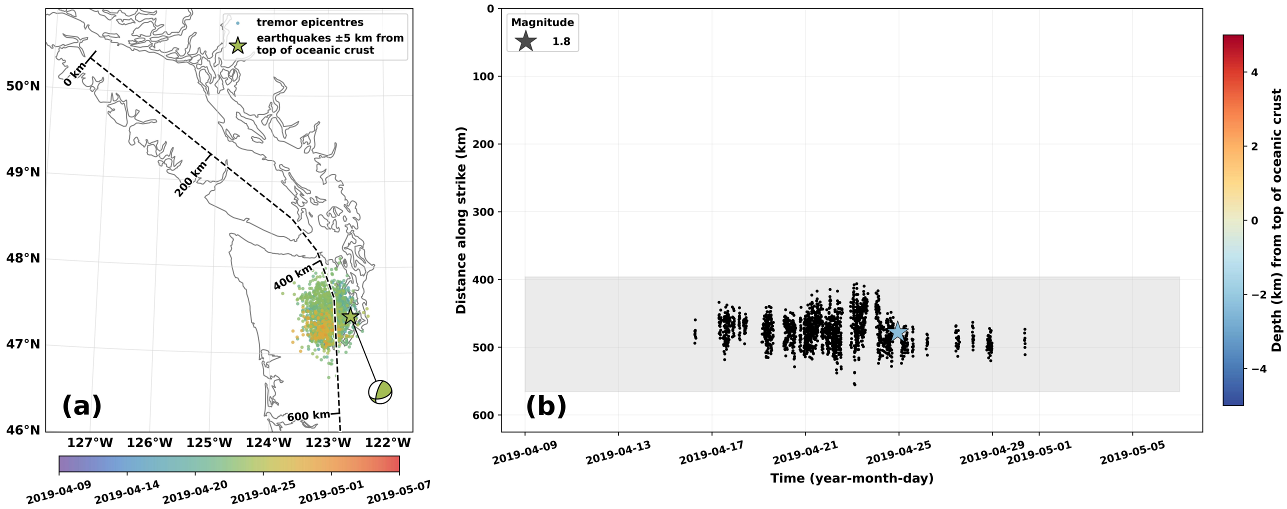

Figure 9 An example of an earthquake occurring within the proximity an ETS event in the southern Puget Sound area in 2019. (a) ETS tremor (dots) began 2019-04-16 and ended 2019-04-30. Tremor is coloured according to time starting seven days before the event and ending seven days after. The earthquake (star) is coloured according to its origin time (2019-04-24 22:38:51 UTC) within that period, with the first-motion focal-mechanism solution provided by PNSN. The PNSN event ID is 61519702. (b) ETS tremor (black dots) over time along strike. Earthquakes (stars) occurring within ±5 km of the top of the subducting plate are coloured according to their depth within that range. The grey shaded rectangle in (b) denotes the period of time and along-strike extent of activity shown in (a).

spectively; Section 3.2). We hypothesize that the difference in earthquake magnitudes before and during/after ETS may be attributed to the degree of tapering in the cumulative distribution for M $\gtrsim$ 2.5. It is worth noting that only 3% of earthquakes in these periods have M $\geq$ 2.5, which represents a difference of 8 earthquakes between the before and after periods, and 11 earthquakes between the before and during periods over the 18 years examined in this study.

The biggest challenge to studying the temporal variation of seismicity in northern Cascadia is that seismicity rates are low. Small absolute changes to low seismicity rates or low occurrence of larger magnitude events can represent large relative changes. For example, a difference of two earthquakes per day represents a 300% increase to the average seismicity rate proximal to ETS (approximately one earthquake per day). In contrast, seismicity proximal to the slow slip area in northern Hikurangi averages 14 earthquakes per day (Yarce et al., 2023). Due to the small-numbers problem, it is difficult to discern whether small variations are robust, even if statistical significance is demonstrated. Previous work in Hikurangi (Yarce et al., 2023) and Cascadia (Morton et al., 2023) demonstrate that catalogues of automatically-located earthquakes can increase detection rates by 4–6 times. Enhanced earthquake catalogues produced with denser seismic networks and automated detection can address the small-numbers problem to some degree, but the effectiveness of these efforts would be limited by actual seismicity rates, which are likely to remain low.

Another major challenge in studying the effects of ETS on seismicity is the significant uncertainty regarding ETS, including (but not limited to) location and structure of the subduction fault in the ETS zone, the mechanisms generating tremor, the processes driving ETS recurrence, the structures hosting ETS activity, and the role of fluids over long and short time scales. These unknowns impose significant analytical limitations and/or require critical assumptions. For example, the association between tremor and slip is reliable over broad spatial and temporal scales, but their relationship over short time scales (hours to days) is not well understood. Some work indicates that peak slip rates lag peak tremor occurrence by 3–5 days (Hall et al., 2019). In addition, it is not known whether the amount of tremor generated during ETS is related to the cumulative slip of the event. Previous estimates indicate that the cumulative seismic (i.e., tremor) moment of ETS is $<$ 0.1% of the cumulative aseismic (i.e., slip) moment (Kao et al., 2010), and the ratio of cumulative tremor energy to average slow slip rates varies along strike and dip (Wech, 2021). If the effects of ETS on seismicity depend on slip magnitudes, as seems to be the case in Hikurangi (Todd et al., 2018), the poorly-understood relationship between tremor occurrence and slip rates/magnitudes limits the effectiveness of using tremor alone in such an analysis.

While this study examines regular earthquakes and ETS using long-term observations, future work may also examine this relationship through case studies. We present here two possible cases that may be of interest for future analysis. In the catalogues employed here, there are 10 ETS events wherein one or more earthquakes occurred within ±5 km of the top of the subducting plate concurrent with tremor. Figure 9 shows an instance where a M1.8 earthquake located by PNSN occurred during an ETS event in the southern Puget Sound area in 2019. Uncertainties on the depth of the earthquake and the location of the megathrust fault do not allow us to confidently conclude whether this event originated on the megathrust. However, with a

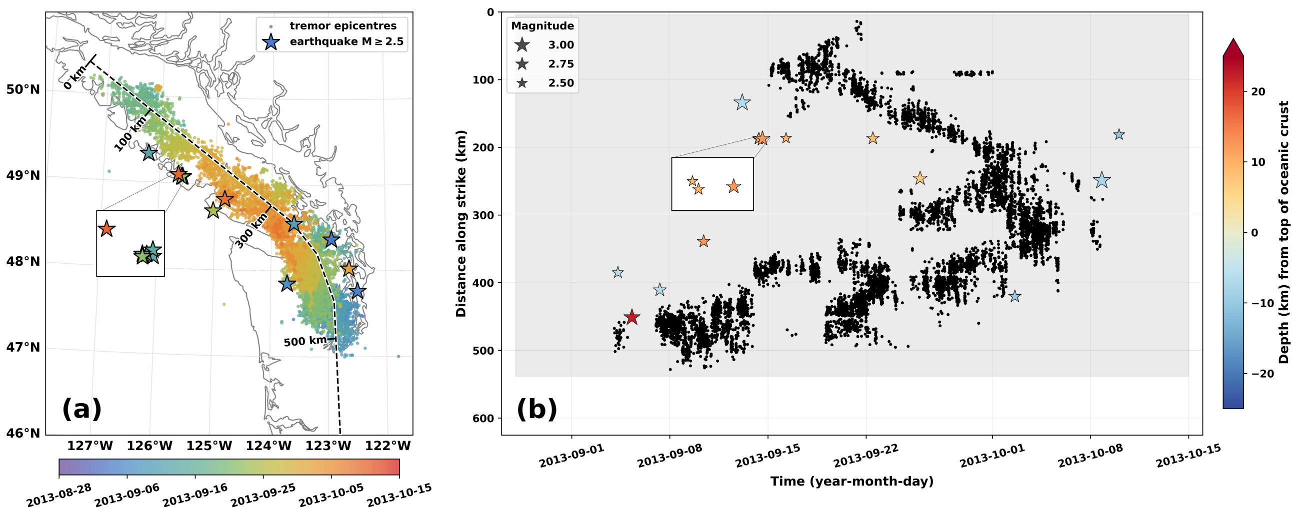

Figure 10 An example of M≥2.5 earthquake activity during a 2013 ETS event. (a) ETS tremor (dots) began 2013-09-04 and ended 2013-10-08. Tremor is coloured according to time starting 7 days before the event and ending 7 days after. Earthquakes (stars) are coloured according to their origin times within that period. (inset a) A zoomed-in area of six earthquakes obscured in the main plot due to overlapping markers. (b) ETS tremor (black dots) over time along strike. Earthquakes M≥2.5 (stars) are coloured according to their depth from the top of the subducting plate. The grey shaded rectangle in (b) denotes the period of time and along-strike extent of activity shown in (a). (inset b) A zoomed-in area of three earthquakes obscured in the main plot due to overlapping markers.

depth of 46.4–2.4 km below the top of the subducting plate model, it is likely that this event was generated in the vicinity of ETS processes, if not on the megathrust fault itself. Focal mechanisms for low-magnitude earthquakes often cannot be computed reliably, but PNSN does provide a focal mechanism solution for this event (Figure 9a), which suggests an oblique thrust mechanism; more analysis is required to determine whether this mechanism is reliable and consistent with subduction at this location.

We similarly find six ETS events wherein one or more earthquakes $M \geq 2.5$ occurred (> 10 km depth) in the vicinity of tremor. Figure 10 shows an instance where 13 earthquakes $M \geq 2.5$ occurred during an ETS event (according to the definition used in Section 3.2) throughout Vancouver Island and Washington in September and October of 2013. These earthquakes—a mix of upper-crust and in-slab events—represent more than one third of all earthquakes $M \geq 2.5$ that occurred during ETS between 2006 and 2024. This ETS event is also the only event in our tremor episode catalogue where tremor initiated at two or more locations along the margin and converged to terminate at one location. Future studies of cases such as these may be opportunities to understand where earthquakes during ETS occur and therefore which faults might be activated by ETS activity, and what specific ETS processes may contribute to these effects.

5 Summary and Conclusions

In this paper, we present a spatial-temporal analysis of seismicity before, during, and after ETS in northern Cascadia. We define spatial-temporal clusters of tremor episodes to represent ETS between 2006 and 2024, and we merge six earthquake catalogues to represent regional seismicity. We show that daily seismicity rates (regional and proximal to ETS) exhibit no statistically-significant temporal variation in association with ETS. We also show that the frequency–magnitude distribution for earthquakes $M \gtrsim 2.5$ in/near the ETS zone is tapered below the best-fit GR law (Figure 3); a taper is not observed for earthquakes during and within 28 days after ETS (Figures 6 and 8). Statistical tests give strong evidence that magnitudes of proximal earthquakes during and after ETS are distinct from those before ETS. There is weak statistical evidence that magnitudes of margin-wide earthquakes during ETS are distinct from those between ETS events. We interpret these results to indicate that seismicity in/near the ETS zone in northern Cascadia is characterized by fewer $M \gtrsim 2.5$ earthquakes than predicted by the GR law (i.e., the distribution is tapered), except during ETS events when $M \gtrsim 2.5$ earthquakes are more numerous such that the observed frequency–magnitude distribution is in good agreement with the GR law.

Several factors make it challenging to study potential links between seismicity and ETS in northern Cascadia, including low seismicity rates and broad unknowns regarding ETS. In light of these challenges, analytical approaches that focus on individual cases may be fruitful. We highlight two instances that are good candidates for future investigation, including: (1) an earthquake in Puget Sound with a depth and focal mechanism potentially indicating slip on the megathrust during ETS (Figure 9); and (2) 13 $M \geq 2.5$ earthquakes that occurred during a single ETS event (Figure 10). This represents 17 times more $M \geq 2.5$ earthquakes than the mean (0.77 $M \geq 2.5$ earthquakes per ETS event) over all other ETS events. The work presented here provides a starting point for future examination of any relationship between ETS and seismicity in Cascadia.

Acknowledgements

Thank you to Dr. Jeremy Gosselin for suggesting an analysis of earthquake magnitude *b*-values. We thank two anonymous reviewers for their interest in this topic and their suggested improvements to this manuscript. Funding for this work is provided by NSERC Discovery Grant RGPIN-2024-04391.

Data and code availability

The NRCan NEDB containing earthquakes in western Canada in 1985–2024 is accessed here: https://www.earthquakescanada.nrcan.gc.ca/fdsnws/event/1/query?starttime=2010-01-01T00:00:00&endtime=2025-01-01T00:00:00&format=text&nodata=404.
The PNSN earthquake catalogue is accessed through a custom search of the database (https://pnsn.org/events?custom_search=true) using latitude and longitude ranges of $45°$ to $49°$ and $-121°$ to $-126.5°$, respectively. Earthquake catalogues in Table 1 referenced to the scientific literature can be accessed from repositories given in their respective articles. Tremor in Cascadia is accessed at the PNSN Tremor Map webpage (https://www.pnsn.org/tremor). Metadata for tremor episodes produced in this study is accessed from Zenodo (https://zenodo.org/records/15692805). Code for computing *b*-values was copied from GitHub (https://github.com/sachalapins/bvalues).

Competing interests

The authors have no competing interests.

References

Aki, K. Maximum likelihood estimate of b in the formula log N=a-bM and its confidence limits. *Bulletin of the Earthquake Research Institute*, 43:237–239, 1965.

Bartlow, N. M. A Long-Term View of Episodic Tremor and Slip in Cascadia. *Geophysical Research Letters*, 47(3), 2020. doi: 10.1029/2019gl085303.

Bloch, W., Bostock, M. G., and Audet, P. A Cascadia Slab Model From Receiver Functions. *Geochemistry, Geophysics, Geosystems*, 24(10), 2023. doi: 10.1029/2023gc011088.

Bombardier, M. Episode Metadata v2 [data set]. Zenodo, 2025. doi: 10.5281/zenodo.15206757.

Bombardier, M., Cassidy, J. F., Dosso, S. E., and Kao, H. Spatial Distribution of Tremor Episodes From Long-Term Monitoring in the Northern Cascadia Subduction Zone. *Journal of Geophysical Research: Solid Earth*, 129(8), 2024. doi: 10.1029/2024jb029159.

Bostock, M. G., Christensen, N. I., and Peacock, S. M. Seismicity in Cascadia. *Lithos*, 332-333:55–66, 2019. doi: 10.1016/j.lithos.2019.02.019.

Boyarko, D., Brudzinski, M., Porritt, R., Allen, R., and Tréhu, A. Automated detection and location of tectonic tremor along the entire Cascadia margin from 2005 to 2011. *Earth and Planetary Science Letters*, 430:160–170, 2015. doi: 10.1016/j.epsl.2015.06.026.

Brudzinski, M. R. and Allen, R. M. Segmentation in episodic tremor and slip all along Cascadia. *Geology*, 35(10):907, 2007. doi: 10.1130/g23740a.1.

Davis, E. E., Sun, T., Heesemann, M., Becker, K., and Schlesinger, A. Long-Term Offshore Borehole Fluid-Pressure Monitoring at the Northern Cascadia Subduction Zone and Inferences Regarding the State of Megathrust Locking. *Geochemistry, Geophysics, Geosystems*, 24(6), 2023. doi: 10.1029/2023gc010910.

Delahaye, E., Townend, J., Reyners, M., and Rogers, G. Microseismicity but no tremor accompanying slow slip in the Hikurangi subduction zone, New Zealand. *Earth and Planetary Science Letters*, 277(1-2):21–28, 2009. doi: 10.1016/j.epsl.2008.09.038.

Dragert, H., Wang, K., and James, T. S. A Silent Slip Event on the Deeper Cascadia Subduction Interface. *Science*, 292(5521): 1525–1528, 2001. doi: 10.1126/science.1060152.

Ester, M., Kriegel, H.-P., Sander, J., and Xu, X. A Density-Based Algorithm for Discovering Clusters in Large Spatial Databases with Noise. In *Proceedings of the Second International Conference on Knowledge Discovery and Data Mining*, KDD'96, page 226–231. AAAI Press, 1996.

Gao, X. and Wang, K. Rheological separation of the megathrust seismogenic zone and episodic tremor and slip. *Nature*, 543 (7645):416–419, 2017. doi: 10.1038/nature21389.

Halchuk, S., Allen, T. I., Rogers, G. C., and Adams, J. *Seismic Hazard Earthquake Epicentre File (SHEEF2010) used in the fifth generation seismic hazard maps of Canada*. 2015. doi: 10.4095/296908.

Hall, K., Schmidt, D., and Houston, H. Peak Tremor Rates Lead Peak Slip Rates During Propagation of Two Large Slow Earthquakes in Cascadia. *Geochemistry, Geophysics, Geosystems*, 20 (11):4665–4675, 2019. doi: 10.1029/2019gc008510.

Hirose, H., Matsuzawa, T., Kimura, T., and Kimura, H. The Boso slow slip events in 2007 and 2011 as a driving process for the accompanying earthquake swarm. *Geophysical Research Letters*, 41 (8):2778–2785, 2014. doi: 10.1002/2014gl059791.

Itoh, Y., Aoki, Y., and Fukuda, J. Imaging evolution of Cascadia slow-slip event using high-rate GPS. *Scientific Reports*, 12(1), 2022. doi: 10.1038/s41598-022-10957-8.

Kao, H., Shan, S., Dragert, H., and Rogers, G. Northern Cascadia episodic tremor and slip: A decade of tremor observations from 1997 to 2007. *Journal of Geophysical Research: Solid Earth*, 114 (B11), 2009. doi: 10.1029/2008jb006046.

Kao, H., Wang, K., Dragert, H., Kao, J. Y., and Rogers, G. Estimating seismic moment magnitude (Mw) of tremor bursts in northern Cascadia: Implications for the "seismic efficiency" of episodic tremor and slip. *Geophysical Research Letters*, 37(19), 2010. doi: 10.1029/2010gl044927.

Kato, A., Obara, K., Igarashi, T., Tsuruoka, H., Nakagawa, S., and Hirata, N. Propagation of Slow Slip Leading Up to the 2011 M_w9.0 Tohoku-Oki Earthquake. *Science*, 335(6069):705–708, 2012. doi: 10.1126/science.1215141.

Kirkpatrick, J. D., Fagereng, A., and Shelly, D. R. Geological constraints on the mechanisms of slow earthquakes. *Nature Reviews Earth & Environment*, 2(4):285–301, 2021. doi: 10.1038/s43017-021-00148-w.

Kita, S., Houston, H., Yabe, S., Tanaka, S., Asano, Y., Shibutani, T., and Suda, N. Effects of episodic slow slip on seismicity and stress near a subduction-zone megathrust. *Nature Communications*, 12(1), 2021. doi: 10.1038/s41467-021-27453-8.

Linde, A. T., Gladwin, M. T., Johnston, M. J. S., Gwyther, R. L., and Bilham, R. G. A slow earthquake sequence on the San Andreas fault. *Nature*, 383(6595):65–68, 1996. doi: 10.1038/383065a0.

Merrill, R., Bostock, M. G., Peacock, S. M., Calvert, A. J., and Christensen, N. I. A Double Difference Tomography Study of the Washington Forearc: Does Siletzia Control Crustal Seismicity? *Journal of Geophysical Research: Solid Earth*, 125(10), 2020. doi: 10.1029/2020jb019750.

Morton, E. A., Bilek, S. L., and Rowe, C. A. Cascadia Subduction Zone Fault Heterogeneities From Newly Detected Small Magnitude Earthquakes. *Journal of Geophysical Research: Solid Earth*, 128(6), 2023. doi: 10.1029/2023jb026607.

Nishikawa, T., Nishimura, T., and Okada, Y. Earthquake Swarm Detection Along the Hikurangi Trench, New Zealand: Insights Into the Relationship Between Seismicity and Slow Slip Events. *Journal of Geophysical Research: Solid Earth*, 126(4), 2021. doi: 10.1029/2020jb020618.

Nishikawa, T., Ide, S., and Nishimura, T. A review on slow earthquakes in the Japan Trench. *Progress in Earth and Planetary Science*, 10(1), 2023. doi: 10.1186/s40645-022-00528-w.

Ozawa, S., Murakami, M., and Tada, T. Time-dependent inversion study of the slow thrust event in the Nankai trough subduction zone, southwestern Japan. *Journal of Geophysical Research: Solid Earth*, 106(B1):787–802, 2001. doi: 10.1029/2000jb900317.

Rogers, G. and Dragert, H. Episodic Tremor and Slip on the Cascadia Subduction Zone: The Chatter of Silent Slip. *Science*, 300 (5627):1942–1943, 2003. doi: 10.1126/science.1084783.

Savard, G., Bostock, M. G., and Christensen, N. I. Seismicity, Metamorphism, and Fluid Evolution Across the Northern Cascadia Fore Arc. *Geochemistry, Geophysics, Geosystems*, 19(6): 1881–1897, 2018. doi: 10.1029/2017gc007417.

Schneider, M., Flury, H., Guttorp, P., and Wright, A. Earthquake Catalog Processing and Swarm Identification for the Pacific Northwest. *Seismological Research Letters*, 94(5):2500–2513, 2023. doi: 10.1785/0220220374.

Schwartz, S. Y. and Rokosky, J. M. Slow slip events and seismic tremor at circum-Pacific subduction zones. *Reviews of Geophysics*, 45(3), 2007. doi: 10.1029/2006rg000208.

Segall, P., Desmarais, E. K., Shelly, D., Miklius, A., and Cervelli, P. Earthquakes triggered by silent slip events on Kīlauea volcano, Hawaii. *Nature*, 442(7098), 2006. doi: 10.1038/nature04938.

Shaddox, H. R. and Schwartz, S. Y. Subducted seamount diverts shallow slow slip to the forearc of the northern Hikurangi subduction zone, New Zealand. *Geology*, 47(5):415–418, 2019. doi: 10.1130/g45810.1.

Shi, Y. and Bolt, B. A. The standard error of the magnitude-frequency b value. *Bulletin of the Seismological Society of America*, 72(5):1677–1687, 1982. doi: 10.1785/bssa0720051677.

Todd, E. K., Schwartz, S. Y., Mochizuki, K., Wallace, L. M., Sheehan, A. F., Webb, S. C., Williams, C. A., Nakai, J., Yarce, J., Fry, B., Henrys, S., and Ito, Y. Earthquakes and Tremor Linked to Seamount Subduction During Shallow Slow Slip at the Hikurangi Margin, New Zealand. *Journal of Geophysical Research: Solid Earth*, 123 (8):6769–6783, 2018. doi: 10.1029/2018jb016136.

Tréhu, A. M., Braunmiller, J., and Nabelek, J. L. Probable low-angle thrust earthquakes on the Juan de Fuca–North America plate boundary. *Geology*, 36(2):127, 2008. doi: 10.1130/g24145a.1.

Vidale, J. E., Hotovec, A. J., Ghosh, A., Creager, K. C., and Gomberg, J. Tiny intraplate earthquakes triggered by nearby episodic tremor and slip in Cascadia. *Geochemistry, Geophysics, Geosystems*, 12(6), 2011. doi: 10.1029/2011gc003559.

Wallace, L. M., Beavan, J., Bannister, S., and Williams, C. Simultaneous long-term and short-term slow slip events at the Hikurangi subduction margin, New Zealand: Implications for processes that control slow slip event occurrence, duration, and migration. *Journal of Geophysical Research: Solid Earth*, 117 (B11), 2012. doi: 10.1029/2012jb009489.

Wech, A. G. Interactive Tremor Monitoring. *Seismological Research Letters*, 81(4):664–669, 2010. doi: 10.1785/gssrl.81.4.664.

Wech, A. G. Cataloging Tectonic Tremor Energy Radiation in the Cascadia Subduction Zone. *Journal of Geophysical Research: Solid Earth*, 126(10), 2021. doi: 10.1029/2021jb022523.

Wech, A. G. and Bartlow, N. M. Slip rate and tremor genesis in Cascadia. *Geophysical Research Letters*, 41(2):392–398, 2014. doi: 10.1002/2013gl058607.

Wech, A. G. and Creager, K. C. Automated detection and location of Cascadia tremor. *Geophysical Research Letters*, 35(20), 2008. doi: 10.1029/2008gl035458.

Wech, A. G. and Creager, K. C. A continuum of stress, strength and slip in the Cascadia subduction zone. *Nature Geoscience*, 4(9): 624–628, 2011. doi: 10.1038/ngeo1215.

Wech, A. G., Creager, K. C., and Melbourne, T. I. Seismic and geodetic constraints on Cascadia slow slip. *Journal of Geophysical Research: Solid Earth*, 114(B10), 2009. doi: 10.1029/2008jb006090.

Wech, A. G., Boese, C. M., Stern, T. A., and Townend, J. Tectonic tremor and deep slow slip on the Alpine Fault. *Geophysical Research Letters*, 39(10), 2012. doi: 10.1029/2012gl051751.

Wiemer, S. and Wyss, M. Minimum Magnitude of Completeness in Earthquake Catalogs: Examples from Alaska, the Western United States, and Japan. *Bulletin of the Seismological Society of America*, 90(4):859–869, 2000. doi: 10.1785/0119990114.

Yamamoto, Y., Yada, S., Ariyoshi, K., Hori, T., and Takahashi, N. Seismicity distribution in the Tonankai and Nankai seismogenic zones and its spatiotemporal relationship with interplate coupling and slow earthquakes. *Progress in Earth and Planetary Science*, 9(1), 2022. doi: 10.1186/s40645-022-00493-4.

Yarce, J., Sheehan, A. F., and Roecker, S. Temporal Relationship of Slow Slip Events and Microearthquake Seismicity: Insights From Earthquake Automatic Detections in the Northern Hikurangi Margin, Aotearoa New Zealand. *Geochemistry, Geophysics, Geosystems*, 24(3), 2023. doi: 10.1029/2022gc010537.